Hindawi
Journal of Engineering
Volume 2022, Article ID 7343984, 17 pages
https://doi.org/10.1155/2022/7343984

Research Article

Prediction of the Radiative Properties of Triangular-Grating Surfaces from Electromagnetic Theory

Taoufik Ghabara

Department of Physics, College of Science and Arts, Qassim University, Ar Rass 51921, Qassim, Saudi Arabia

Correspondence should be addressed to Taoufik Ghabara; taoufikghabara@gmail.com

Received 29 April 2022; Revised 19 September 2022; Accepted 29 September 2022; Published 26 October 2022

Academic Editor: Oronzio Manca

In this paper, we present a study of the influence of roughness on the bidirectional reflectivity and on the emissivity of surfaces using Maxwell's electromagnetic theory. In this framework, we solve the Helmholtz equations by using the surface integral method. We first proceed to a general description of this method, allowing to solve the propagation equations of the electromagnetic field. We then express the diffused directional flux using the surface field and its normal derivative (source terms), in the case of an incident plane wave in "p" polarization or in "s" polarization. This finally allows us to arrive at the desired radiative properties. We have developed two numerical calculation codes whose use we limit to cases of surfaces presenting cavities in the shape of a symmetrical or asymmetrical "V". Particular interest was given to the influence of the geometric parameters of these surfaces on the bidirectional reflection function and on the emissivity of these surfaces. Finally, we present some very conclusive results.

1. Introduction

The theoretical or experimental determination of the radiative properties of rough surfaces is the subject of several research works. These parameters are involved in very varied fields of application ranging from the calculation of energy exchanges by thermal radiation to the design of selective rough surfaces, in addition to common applications in concentrated solar power, agriculture, medicine, radar waves, etc. A better understanding of the physical phenomena related to the interaction of electromagnetic waves with a surface is always necessary to master the problem. Different numerical simulation models to study these radiative properties have been developed. When the surface is made up of asperities with a characteristic dimension greater than the wavelength, it is said to be macrorough. In this case, among the study methods used, we cite the iterative method, the variational method, the Monte-Carlo statistical method, and the image method [1–4]. In the case of microrough surface, methods based on notions of physical optics are developed and applied [4]; a particular interest is then focused on the energy reflected in a coherent or incoherent way.

More recently, models based essentially on Maxwell's equations and the integral surface method have made it possible to study the diffusion of electromagnetic waves by rough surfaces. In this context, we cite the work of Grefet [5], Greffet and Ladan [6], and Ladan and Buckius [7] as well as the diversified and highly enriching work of Buckius et al. [8–11] and Charles et al. [12]. The interest of these authors is particularly focused on the study of the bidirectional reflectivity or the emissivity of random or regular rough surfaces of a conductive or dielectric material. Most often, these surfaces are illuminated by a plane wave [13] or by an incident Gaussian beam [7]. The results are analyzed in the two cases of polarization "p" and "s," that is, parallel and perpendicular. It should also be noted that experimental work is carried out in order to validate the various models developed [14–16].

In the present work, we propose to contribute to the study of the influence of a roughness in the shape of symmetrical or asymmetrical "V," on the bidirectional

reflectivity and on the emissivity of these surfaces using Maxwell's electromagnetic theory. In this context, the Helmholtz equations are solved by the application of the surface integral method. We have limited the exploitation of these numerical calculation codes to the cases of surfaces presenting cavities in the shape of a symmetrical or asymmetrical "V." The material constituting the studied surface being $BaSO_4$, with a complex refractive index $n_c = 1,628 + i0,0003$ corresponding to the wavelength $\lambda = 0,6328\mu m$.

Particular interest was given to the influence of the geometric parameters of these surfaces on the bidirectional reflection function and on the emissivity of these surfaces.

2. Determination of Radiative Properties by using the Surface Integral Method

2.1. Incident Field. We consider in our work a surface presenting longitudinal cavities contiguous in the form of symmetrical or asymmetrical "V." In the section plane (xOz), the profile of this surface is represented by a periodic function ξ of the variable x; this is characterized by its geometric period λ_1, its height h, and a parameter f_0, between 0 and 1, indicating the position of the peak of the surface. These cavities are dug on the surface of a homogeneous, linear, and isotropic dielectric medium Ω_2, with a complex refractive index n_c. We designate by Ω_1 the half-space defined by$z > \xi(x)$ and assimilated to the void. We work with an incident plane wave at the angle θ_0 in both cases of polarization. The first concerns the "p" polarization, for which the magnetic excitation field $\vec{H}$ is perpendicular to the plane of incidence (xOz), and it is expressed in vacuum at a point M $(x, 0, z)$ by:

$$\vec{H}(x,z) = H_y \vec{e}_y = H_y(x,z)\vec{e}_y, \tag{1}$$

with:

$$H_y(x,z) = H_0 \exp\{iK_0(x\sin\theta_0 - z\cos\theta_0)\}, \tag{2}$$

where H0 is the amplitude of the magnetic field and $K_0 = \omega/c$ is the wave number.

The second case concerns the "s" polarization, for which the incident electric $\vec{E}$ field is perpendicular to this plane. Case development will not be presented in this paper.

2.2. Helmholtz Equations in "p" Polarization. We denote by $H_y^{>}(x,z)$ the field evaluated at an observation point of coordinates x and $z > \xi(x)$, located in a vacuum. This field obeys the Helmholtz equation:

$$\Delta H_y^{>}(x,z) + K_0^2 H_y^{>}(x,z) = 0, \quad \text{pour } z > \xi(x), \tag{3}$$

and checks an outgoing wave condition at infinity.

The field $H_y^{<}(x,z)$ in the medium Ω_2 evaluated at a point of coordinates x and $z < \xi(x)$ obeys the equation:

$$\Delta H_y^{<}(x,z) + \varepsilon_r(\omega) K_0^2 H_y^{<}(x,z) = 0 \quad \text{pour } z < \xi(x), \tag{4}$$

or $\varepsilon_r = n_c^2$. This field decreases exponentially when z tends to $-\infty$.

The surface passage conditions $\xi(x)$ are as follows:

$$H_y^{>}(x,z)|_{z=\xi^+(x)} = H_y^{<}(x,z)|_{z=\xi^-(x)}. \tag{5}$$

$$\frac{\partial H_y^{>}(x,z)}{\partial n}\Big|_{z=\xi^+(x)} = \frac{1}{\varepsilon_r}\frac{\partial H_y^{<}(x,z)}{\partial n}\Big|_{z=\xi^-(x)}, \tag{6}$$

where $\xi^+(x)$ is the ordinate of the abscissa point x, which tends towards the surface while remaining in the middle Ω_1. Whereas, $\xi^-(x)$ is the ordinate of the abscissa point x which tends towards the surface while remaining in the middle Ω_2. $\partial/\partial n$ designates the partial derivative along the normal, to the surface at the point $(x, z = \xi(x))$. The normal unit vector at the interface, oriented from Ω_2 towards Ω_1, is defined as follows:

$$\vec{n} = \left(\frac{1}{\gamma}\right)\left(-\frac{\mathrm{d}[\xi(x)]}{\mathrm{d}x}, 0, 1\right), \tag{7}$$

with:

$$\gamma = \left[1 + \left\{\frac{\mathrm{d}[\xi(x)]}{\mathrm{d}x}\right\}^2\right]^{1/2}, \tag{8}$$

the expression of the derivative following the normal is written as follows:

$$\frac{\partial}{\partial n} = \left[1 + \left[\xi^{\copyright}(x)\right]^2\right]^{-(1/2)}\left(-\xi'(x)\frac{\partial}{\partial x} + \frac{\partial}{\partial z}\right). \tag{9}$$

For an oriented normal of Ω_1 to Ω_2, the expression of the derivative is written as follows:

$$\frac{\partial}{\partial n'} = -\frac{\partial}{\partial n}. \tag{10}$$

2.3. Integral Surface Equations in "p" Polarization

2.3.1. Integral Equations of the Field above the Interface. Having introduced Green's functions [1,2], we now apply Helmholtz's theorem to the differential equation (3). For this, we choose the volume $\widetilde{V}$ limited by the closed surface $\partial\widetilde{V}$ and located above the interface $(z > \xi(x))$. We can write for the field $H_y^{>}$ the following equations:

$$H_y^{>}(r) = \frac{1}{4\pi}\int_{\partial\widetilde{v}}\left[G_0 \nabla_{r'} H_y^{>} - H_y^{>} \nabla_{r'} G_0\right]\mathrm{d}S \quad si\, M \in \widetilde{v}. \tag{11}$$

$$\frac{1}{4\pi}\int_{\partial\widetilde{v}}\left[G_0 \nabla_{r'} H_y^{>} - H_y^{>} \nabla_{r'} G_0\right]\mathrm{d}S = 0 \quad si\, M \notin \widetilde{v}, \tag{12}$$

where $(\widetilde{V})$ is the volume bounded by the closed surface $(\partial\widetilde{V})$ and $\partial/\partial n$ denotes the derivative along the outgoing normal. Subdivide the surface $\partial\widetilde{V}$ into two parts, one $\sum_1^+$ located just above the interface $(z = \xi(x) + \alpha, \quad \text{avec } \alpha \longrightarrow 0^+)$ and the other $\sum_2^+$ closing on $\widetilde{V}$. The surface integral in (7) is then written as the sum of the integrals over the surfaces $\sum_1^+$ et $\sum_2^+$: $\int_{\partial\widetilde{V}}\mathrm{d}S = \int_{\sum_1^+}\mathrm{d}S + \int_{\sum_2^+}\mathrm{d}S$. By tending $\sum_2^+$ to a hemispherical surface $\sum^{(+\infty)^\circ}$ of infinite radius located

in Ω_1, and taking into account the Sommerfeld condition [3], we get the following:

$$\int_{\sum}{}_{(+\infty)}\left[G_0\frac{\partial H_y^{>}}{\partial n'}-H_y^{>}\frac{\partial G_0}{\partial n'}\right]\mathrm{d}S=4\pi H_{\mathrm{yinc}}^{>}. \tag{13}$$

Using Cartesian coordinates, the expression for the integral (7) becomes:

$$H_y^{>}(x,z)=H_{\mathrm{yinc}}^{>}(x,z)+\frac{1}{4\pi}\int_{\sum_1^+}\left[G_0\frac{\partial H_y^{>}}{\partial n'}-H_y^{>}\frac{\partial G_0}{\partial n'}\right]\mathrm{d}S. \tag{14}$$

Let us express the surface element dS. For this, we denote by s the curvilinear abscissa on the profile, and the elementary displacement on the latter is written as $\mathrm{d}\vec{S}=[-\xi'(x)\vec{e}_x+\vec{e}_z]\mathrm{d}x$. The relations (7) and (8) expressing lead to:

$$\mathrm{d}S=\|\mathrm{d}\vec{S}\|=\gamma\mathrm{d}x. \tag{15}$$

Given (10), equation (14) can then be written in the following form:

$$H_y^{>}(x,z)=H_{\mathrm{yinc}}^{>}(x,z)+\frac{1}{4\pi}\int_{-\infty}^{+\infty}\left\{\left[\left(-\xi'(x')\frac{\partial}{\partial x'}+\frac{\partial}{\partial z'}\right)G_0(x,z;x',z')\right]\frac{H_y^{>}(x',z')}{z'=\xi(x')}-G_0(x,z;x',z')\frac{\partial}{\partial n'}\frac{H_y^{>}(x',z')}{z'=\xi(x')}\right\}\mathrm{d}x'. \tag{16}$$

We introduce at this level the source terms H and L defined by:

$$H(x)=H_y^{>}(x,z)|_{z=\xi(x)}, \tag{17}$$

$$L(x)=\frac{\partial}{\partial n}H_y^{>}(x,z)|_{z=\xi(x)}. \tag{18}$$

Physically, H (x) is the magnetic field at the coordinate point $(x,\xi(x)^{>})$ and L (x) represents, up to a constant, the tangential component to the surface of the electric field at this point. We finally arrive at the following equations:

$$\begin{aligned}H_y^{>}(x,z)&=H_{\mathrm{yinc}}^{>}(x,z)+\frac{1}{4\pi}\int_{-\infty}^{+\infty}\left\{\left[\left(-\xi'(x')\frac{\partial}{\partial x'}+\frac{\partial}{\partial z'}\right)G_0(x,z;x',z')\right]\times H(x')|_{z'=\xi(x')}-G_0(x,z;x',z')\times L(x')|_{z'=\xi(x')}\right\}\mathrm{d}x'\ M\in\bar{V},\\ 0&=H_{\mathrm{yinc}}^{>}(x,z)+\frac{1}{4\pi}\int_{-\infty}^{+\infty}\left\{\left[\left(-\xi'(x')\frac{\partial}{\partial x'}+\frac{\partial}{\partial z'}\right)G_0(x,z;x',z')\right]\times H(x')|_{z'=\xi(x')}-G_0(x,z;x',z')\times L(x')|_{z'=\xi(x')}\right\}\mathrm{d}x'\ M\notin\bar{V}.\end{aligned} \tag{19}$$

translating the integral expressions of surface of the field $H_y^{>}(x,z)$ in the vacuum.

2.3.2. Integral Equations of the Field below the Interface. A reasoning analogous to that used in the previous paragraph, applied to G_ε and $H_y^{<}$ the volume $V(z<\xi(x))$ limited by the surface ∂V located just below the interface $\xi(x)$ and closing in Ω_2, provides us with the two other equations which translate the field transmitted into the dielectric. To transform relation (4) into areal integral equations, we apply Helmholtz's theorem, which allows us to write the following equations:

$$H_y^{<}(\vec{r})=\frac{1}{4\pi}\int_{\partial V}\left[G_\varepsilon\frac{\partial H_y^{<}}{\partial n}-H_y^{<}\frac{\partial G_\varepsilon}{\partial n}\right]\mathrm{d}S\ M\in V. \tag{20}$$

$$0=\frac{1}{4\pi}\int_{\partial V}\left[G_\varepsilon\frac{\partial H_y^{<}}{\partial n}-H_y^{<}\frac{\partial G_\varepsilon}{\partial n}\right]\mathrm{d}S\ M\notin V. \tag{21}$$

The surface ∂V is the meeting of two parts, one $\sum_1^-$ located just below the profile $(z=\xi(x)+\alpha,\text{and}\,\alpha\longrightarrow 0^-)$ and the other $\sum_2^-$ closing on V. We tend $\sum_2^-$ towards a surface $\sum^{(-\infty)}$ of infinite radius and located in the middle Ω_2.

We will take into account that there is no incident field for $z<\xi(x)$ and that the field transmitted in the dielectric $[H_y^{<}(x,z)]$ verifies the Sommerfeld condition; so it comes:

$$\int_{\sum}{}_{(-\infty)}\left[G_\varepsilon\frac{\partial H_y^{<}}{\partial n}-H_y^{<}\frac{\partial G_\varepsilon}{\partial n}\right]\mathrm{d}S=0. \tag{22}$$

It follows that the integral (20) can be written in the following form:

$$H_y^{<}(x,z)=\frac{1}{4\pi}\int_{\sum_1^-}\left[G_\varepsilon\frac{\partial H_y^{<}}{\partial n'}-H_y^{<}\frac{\partial G_\varepsilon}{\partial n'}\right]\mathrm{d}S, \tag{23}$$

or:

Table 1: The validity of the model in terms of power in the two cases of polarization.

Polarization	R_{model}	F_{resnel}
Polarization (P)	0,04848535	0,04820009
Polarization (S)	0,06633675	0,0686283

$$H_y^{<}(x,z) = -\frac{1}{4\pi}\int\sum_{1}^{-}\left[H_y^{<}\frac{\partial G_\varepsilon}{\partial n'} - G_\varepsilon\frac{\partial H_y^{<}}{\partial n'}\right]\mathrm{d}S. \tag{24}$$

Using the continuity relations at the interface (5) and (6), this last equation is then written as follows:

$$H_y^{<}(x,z) = -\frac{1}{4\pi}\int\sum_{2}\frac{\left[\left(\partial G_\varepsilon/\partial n\right)H_y^{>} - \varepsilon_r G_\varepsilon\left(\partial H_y^{>}/\partial n\right)\right]}{z=\xi(x)}\mathrm{d}S. \tag{25}$$

By introducing the source terms given by relations (17) and (18), we end up with the following expressions:

$$H_y^{<}(x,z) = -\frac{1}{4\pi}\int_{-\infty}^{+\infty}\left\{\left[\left(-\xi'(x')\frac{\partial}{\partial x'} + \frac{\partial}{\partial z'}\right)G_\varepsilon(x,z;x',z')\right]_{z'=\xi(x')}\times H(x') - \left[\varepsilon_r(\omega)G_\varepsilon(x,z;x',z')\times L(x')\right]_{z'=(x')}\right\}\mathrm{d}x' \text{ for } M\notin V, \tag{26}$$

$$0 = -\frac{1}{4\pi}\int_{-\infty}^{+\infty}\left\{\left[\left(-\xi'(x')\frac{\partial}{\partial x'} + \frac{\partial}{\partial z'}\right)G_\varepsilon(x,z;x',z')\right]_{z'=\xi(x')}\times H(x') - \left[\varepsilon_r(\omega)G_\varepsilon(x,z;x',z')\times L(x')\right]_{z'=(x')}\right\}\mathrm{d}x' \quad \text{for } M\notin V, \tag{27}$$

translating the surface integral equations of the field $H_y^{<}(x,z)$ in the medium Ω_2.

2.4. Bidirectional Reflection Function. We show using equation (7), and the Fourier representation of G_0 [2] and taking $z > \xi_{\max}$, that the scattered magnetic field can be put in the following form:

$$\begin{aligned} H_{y\,\text{diff}}^{>}(x,z) &= \int_{-\infty}^{+\infty}\frac{dk}{2\pi}R_p(k\omega)\exp\left(ikx + i\alpha_0(k\omega)z\right),\\ R_p(k\omega) &= \frac{i}{2\alpha_0(k\omega)}\int_{-\infty}^{+\infty}\left\{\exp\left(-ikx - i\alpha_0(k\omega)\xi(x)\right)\times\left\{i\left[k\xi'(x) - \alpha_0(k\omega)\right]H(x) - L(x)\right\}\mathrm{d}x.\end{aligned} \tag{28}$$

By introducing the Poynting vector [4], and using relation (11), we express the diffused flux around θ_r (reflection angle) in the elementary angle $d\theta_r$:

$$p_{\text{diff}}(\theta_r) = \frac{dP_{\text{diff}}(\theta_r)}{d\theta_r} = l_y\frac{1}{2\omega\varepsilon_0}\frac{1}{8\pi}\left|r_p(\theta_r)\right|^2, \tag{29}$$

where l_y is the width of the surface along the axis (oy) and $r_p(\theta_r)$ is expressed by the following relation:

$$r_p(\theta_r) = \int_{-\infty}^{+\infty}\left\{\exp\left(-iK_0(x)\sin\theta_r + \xi(x)\cos\theta_r\right)\right)\times\left\{iK_0\left[\xi'(x)\sin\theta_r - \cos\theta_r\right]H(x) - L(x)\right\}\mathrm{d}x. \tag{30}$$

We deduce the two-way reflection function [5]:

$$\rho''_{\lambda p}(\theta_0,\theta_r) = \frac{1}{8}\frac{c}{\omega}\frac{1}{l_x\cos\theta_r\cos\theta_0}\left|r_p(\theta_r)\right|^2. \tag{31}$$

A calculation analogous to that of the case of the "p" polarization allows us to write the bidirectional reflection function in "s" polarization:

$$\rho''_{\lambda s}(\theta_0,\theta_r) = \frac{1}{8}\frac{1}{K_0}\frac{1}{l_x\cos\theta_r\cos\theta_0}\left|r_s(\theta_r)\right|^2, \tag{32}$$

or:

$$r_s(\theta_r) = \int_{-\infty}^{+\infty} \{\exp(-iK_0(x\sin\theta_r + \xi(x)\cos\theta_r)) \times \{iK_0[\xi'(x)\sin\theta_r - \cos\theta_r]E(x) - F(x)\}\mathrm{d}x. \quad (33)$$

Note that in this case of polarization, the source functions are defined by the following equation:

$$E(x) = E_y^{>}(x,z)|_{z=\xi(x)};$$
$$F(x) = \left(-\xi(x)\frac{\partial}{\partial x} + \frac{\partial}{\partial z}\right)E_y^{>}(x,z)|_{z=\xi(x)}. \quad (34)$$

2.5. Directional Monochromatic Emissivity. In the case of an opaque surface, knowledge of the hemispherical directional monochromatic reflectivity ρ'_λ leads to that of the directional monochromatic emissivity from the relationship:

$$\varepsilon'_\lambda(\Delta) = 1 - \rho'_\lambda(\Delta). \quad (35)$$

3. Description of the Numerical Resolution Method

In order to calculate these source terms, we consider equations (26) and (27) by taking the observation point of coordinates (x, z) on the upper surface, that is, $z = \xi(x) + \alpha$ with α an infinitely small real. The two integral equations (26) and (27) are then written, respectively, in the following forms:

$$H(x) = H_{\mathrm{inc}}(x) + \int_{-\infty}^{+\infty}[H_0(x,x')H(x') - L_0(x,x')L(x')]\mathrm{d}x', \quad (36)$$

$$0 = -\int_{-\infty}^{+\infty}[H_\varepsilon(x')H(x') - \varepsilon_r(\omega)L_\varepsilon(x,x')L(x')]\mathrm{d}x', \quad (37)$$

where:

$$H(x) = H_y^{>}(x,\xi(x)),$$
$$H_{\mathrm{inc}}(x) = H_{\mathrm{yinc}}^{>}(x,\xi(x)), \quad (38)$$

and where:

$$H_\varepsilon(x,x') = \lim\left[\frac{1}{4\pi}\left(-\xi'(x')\frac{\partial}{\partial x'} + \frac{\partial}{\partial z'}\right) \times G_\varepsilon(x,z;x',z')|_{z'=\xi(x');z=\xi(x)+\alpha}\right]\alpha \longrightarrow 0^+$$
$$= \lim\left[\left(-\frac{i}{4}\right)n_c^2\frac{\omega^2}{c^2} \times \frac{H_1^{(1)}(n_c(\omega)(\omega/c))\left[(x-x')^2 + (\xi(x)-\xi(x')+\alpha)^2\right]^{1/2}}{n_c(\omega/c)\left[(x-x')^2 + (\xi(x)-\xi(x')+\alpha)^2\right]^{1/2}} \times [(x-x')\xi'(x') - (\xi(x)-\xi(x')+\alpha)]\right]\alpha \longrightarrow 0^+,$$
$$L_\varepsilon(x,x') = \lim\frac{1}{4\pi}G_\varepsilon(x,\xi(x)+\alpha,x',\xi(x'))\alpha \longrightarrow 0^+$$
$$= \lim\frac{i}{4}H_0^{(1)}\left[n_c\frac{\omega}{c}\left[(x-x')^2 + (\xi(x)-\xi(x')+\alpha)^2\right]^{1/2}\right]\alpha \longrightarrow 0^+. \quad (39)$$

3.1. Transformation of Integral Equations into Linear Systems. We propose to transform the two integral equations of the source terms into a linear system of equations where the unknowns are H and L. For this, we replace the infinite integrals by integrals limited to the interval $[-(l_x/2), (l_x/2)]$. We divide the latter in N intervals of the same extent and whose centers have for abscissas given by:

$$x_n = -\frac{l_x}{2} + \left(n - \frac{1}{2}\right)\Delta x \quad n = 1, 2, \ldots N, \quad (40)$$

where: $\Delta x = l_x/N$

It follows that equation (36) takes the following form:

$$H(x) = H_{inc}(x) + \sum_{n=1}^{n=N}\int_{x_n-(1/2)\Delta x}^{x_n+(1/2)\Delta x}[H_0(x,x')H(x') - L_0(x,x')L(x')]\mathrm{d}x'. \quad (41)$$

By adopting the hypothesis of a very small variation of H (x) and L (x) on each of the intervals $[x_n - (1/2)\Delta x, x_n + (1/2)\Delta x]$, we can approximate equation (41) by:

$$H(x) = H_{\text{inc}}(x) + \sum_{n=1}^{n=N} \left\{ H(x_n) \int_{x_n-(1/2)\Delta x}^{x_n+(1/2)\Delta x} H_0(x, x')\mathrm{d}x' - L(x_n) \int_{x_n-(1/2)\Delta x}^{x_n+(1/2)\Delta x} L_0(x, x')\mathrm{d}x' \right\}. \tag{42}$$

So taking $x = x_m$ we get:

$$H(x_m) = H_{\text{inc}}(x_m) + \sum_{n=1}^{n=N} \left\{ H(x_n) \int_{x_n-(1/2)\Delta x}^{x_n+(1/2)\Delta x} H_0(x_m, x')\mathrm{d}x' - L(x_n) \int_{x_n-(1/2)\Delta x}^{x_n+(1/2)\Delta x} L_0(x_m, x')\mathrm{d}x' \right\}, \tag{43}$$

where:

$$H_{mn}^{(0)} = \int_{x_n-(1/2)\Delta x}^{x_n+(1/2)\Delta x} H_0(x_m, x')\mathrm{d}x', \tag{44}$$

and:

$$L_{mn}^{(0)} = \int_{x_n-(1/2)\Delta x}^{x_n+(1/2)\Delta x} L_0(x_m, x')\mathrm{d}x'. \tag{45}$$

We obtain:

$$H(x_m) = H_{\text{inc}}(x_m) + \sum_{n=1}^{n=N} \left[H_{mn}^{(0)} H(x_n) - L_{mn}^{(0)} L(x_n) \right]. \tag{46}$$

Similarly, equation (37) takes the following form:

$$\sum_{n=1}^{n=N} \left[H_{mn}^{(\varepsilon)} H(x_n) - \varepsilon(\omega) L_{mn}^{(\varepsilon)} L(x_n) \right] = 0, \tag{47}$$

with:

$$H_{mn}^{(\varepsilon)} = \int_{x_n-(1/2)\Delta x}^{x_n+(1/2)\Delta x} H_\varepsilon(x_m, x')\mathrm{d}x', \tag{48}$$

and:

$$L_{mn}^{(\varepsilon)} = \int_{x_n-(1/2)\Delta x}^{x_n+(1/2)\Delta x} L_\varepsilon(x_m, x')\mathrm{d}x'. \tag{49}$$

Equations (44) and (45) constitute a system with 2N equations and 2N unknowns $H(x_n)$ et $L(x_n)$ with n ranging from 1 to N. The calculation of the coefficients $L_{mn}^{(0)}, H_{mn}^{(0)}, L_{mn}^{(\varepsilon)}, H_{mn}^{(\varepsilon)}$ of this system is presented in the appendix. It appears that:

$$\begin{aligned} H_{mn}^{(\varepsilon)} &= \frac{1}{2}\delta_{mn} + \frac{1}{2}h_{mn}^{(\varepsilon)}, \\ L_{mn}^{(\varepsilon)} &= \frac{1}{2}l_{mn}^{(\varepsilon)}, \end{aligned} \tag{50}$$

where δ_{mn} denotes the Kronecker symbol, and with:

$$h_{mn}^{(\varepsilon)} = \begin{cases} \Delta x\left(-\dfrac{i}{2}\right) n_c^2 \dfrac{\omega^2}{c^2} \times \dfrac{H_1^{(1)}\left\{ n_c(\omega/c)\left[(x_m - x_n)^2 + (\xi(x_m) - \xi(x_n))^2 \right]^{1/2} \right\}}{n_c(\omega/c)\left[(x_m - x_n)^2 + (\xi(x_m) - \xi(x_n))^2 \right]^{1/2}} \\ \times \left[(x_m - x_n)\xi'(x_n) - (\xi(x_m) - \xi(x_n)) \right]; m \neq n \\ \Delta x \dfrac{\xi''(x_m)}{2\pi\gamma_m^2}; m = n, \end{cases} \tag{51}$$

and:

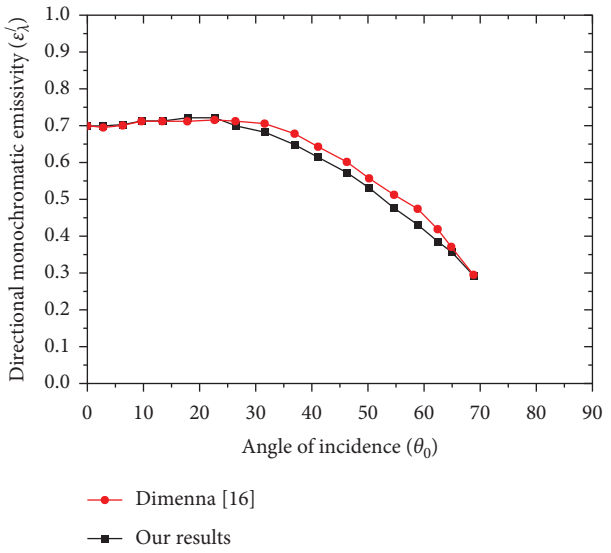

Figure 1: Directional emissivity monochromatic polarization s ($\lambda = 0.6328\mu m$, Sillicon ($n_c = 2.0 + 4.0i$), $h = \lambda, \lambda_1 = \lambda, f_0 = 0.5$).

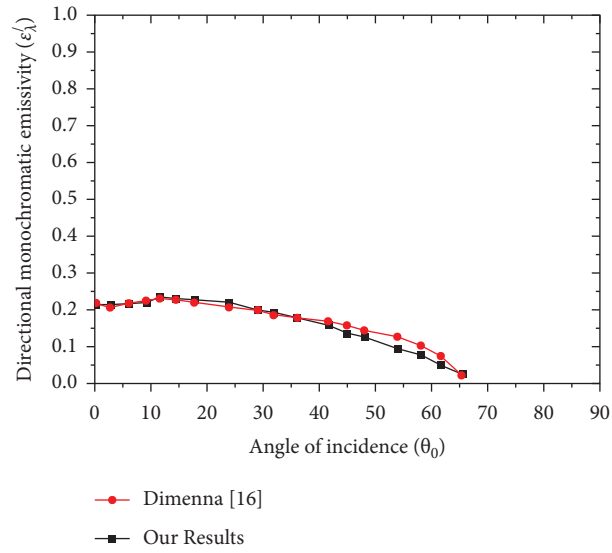

Figure 2: Directional emissivity monochromatic polarization s ($\lambda = 0.6328\mu m$, Alluminum ($n_c = 1.5 + 10.0i$), $h = \lambda, \lambda_1 = \lambda, f_0 = 0.5$).

$$l_{mn}^{(\varepsilon)} = \begin{cases} \Delta x\left(\frac{i}{2}\right) H_0^{(1)}\left\{n_c \frac{\omega}{c}\left[(x_m - x_n)^2 + (\xi(x_m) - \xi(x_n))^2\right]^{1/2}\right\}; m \neq n, \\ \Delta x\left(\frac{i}{2}\right) H_0^{(1)}\left\{n_c \frac{\omega}{c} \frac{\gamma_m \Delta x}{2e}\right\}; m = n, \end{cases} \tag{52}$$

where: $\gamma_m = [1 + (\xi'(x_m)^2)]^{1/2}$ et $n_c = \sqrt{\varepsilon_r}$,

The system of equations (46) and (47) therefore becomes:

$$H(x_m) - \sum_{n=1}^{n=N} \left[h_{mn}^{(0)} H(x_n) - l_{mn}^{(0)} L(x_n)\right] = 2H_{\text{inc}}(x_m),$$
$$H(x_m) + \sum_{n=1}^{n=N} \left[h_{mn}^{(\varepsilon)} H(x_n) - \varepsilon_r(\omega) l_{mn}^{(\varepsilon)} L(x_n)\right] = 0. \tag{53}$$

It can be put in the following matrix form:

$$\begin{pmatrix} \mathbf{I}d - h^{(\mathbf{0})} & \mathbf{l}^{(\mathbf{0})} \\ \mathbf{I}d + \mathbf{h}^{(\varepsilon)} & -\varepsilon(\boldsymbol{\omega}) l^{(\varepsilon)} \end{pmatrix} \times \begin{pmatrix} \mathbf{H} \\ \mathbf{L} \end{pmatrix} = \mathbf{2}\begin{pmatrix} \mathbf{H_{inc}} \\ \mathbf{0} \end{pmatrix}. \tag{54}$$

Or $Id - h^{(0)}, Id + h^{(\varepsilon)}, l^{(0)}, l^{(\varepsilon)}$ denote square blocks consisting of the respective matrix elements $\delta_{mn} - h_{mn}^{(0)}$, $\delta_{mn} - h_{mn}^{(\varepsilon)}, l_{mn}^{(0)}$ et $l_{mn}^{(\varepsilon)}$ [2], and H, L, and H_{inc}, respectively, represent the N components $H(x_k), L(x_k), H_{\text{inc}}(x_k)$.

A similar reasoning allows us to arrive at a linear system with 2N equations and 2N unknowns $E(x_n)$ and $F(x_n)$, components of the source terms in "s" polarization. The numerical resolution of the two linear systems makes it possible to arrive at the source terms in the two cases of polarization. These terms are necessary for the calculations of r_p and r_s expressed by the relations (13) and (15). We replace these with the following expressions:

$$r_p(\theta_r) = \sum_{n=1}^{n=N} \Delta x \times \exp\left[-iK_0(x_n \sin\theta_r + \xi(x_n)\cos\theta_r)\right] \times \left\{iK_0(\xi'(x_n)\sin\theta_r - \cos\theta_r) H(x_n) - L(x_n)\right\},$$
$$r_s(\theta_r) = \sum_{n=1}^{n=N} \Delta x \exp\left[-iK_0(x_n \sin\theta_r + \xi(x_n)\cos\theta_r)\right] \times \left\{iK_0(\xi'(x_n)\sin\theta_r - \cos\theta_r) E(x_n) - F(x_n)\right\}. \tag{55}$$

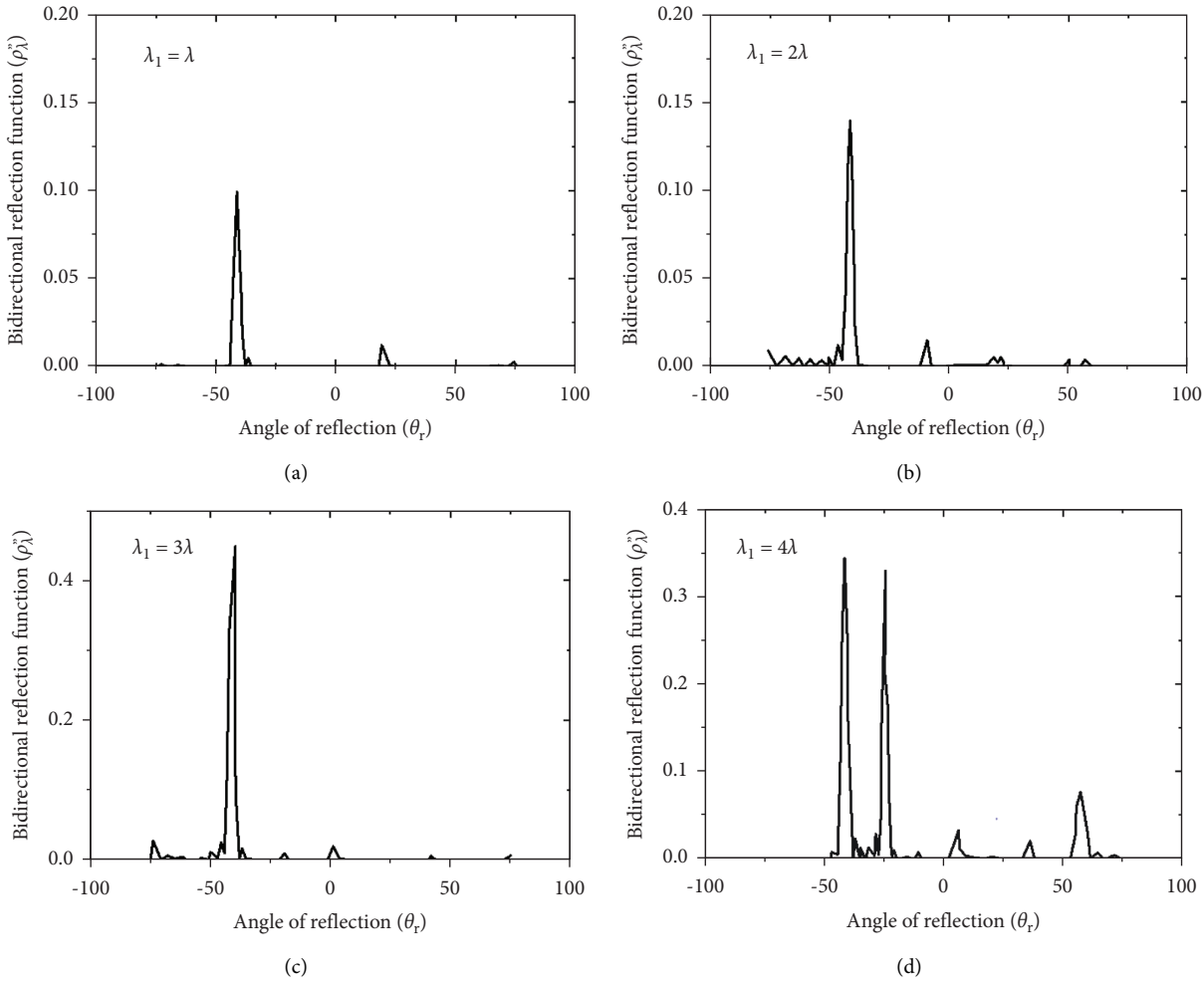

Figure 3: Bidirectional reflection function of polarization p. Influence of the geometric period ($\lambda = 0.6328\mu m, n_c = 1.628 + 0.0003i, \theta_0 = 20^0, h = \lambda, f_0 = 0.5$).

3.2. Model Validation

3.2.1. Validation in terms of Power. We carried out a validation of the developed model, based on a comparison between the ratio of the reflected power to the incident power, calculated using our model with that provided by the Fresnel formulas. As part of this validation, we consider the case of a plane wave and a plane surface for the two kinds of polarization. We note there that the average value along the surface of each of these polarizations is identical to that provided by the formulas of Fresnel (see Table 1).

3.2.2. Validation in terms of Emissivity. We also find the curves provided by Dieenna and Buckius [16] in the case of both silicon and aluminum surfaces for various surface parameters (Figures 1 and 2).

The surfaces are constructed using a Fourier series representation from the surface. The number of terms in the series must be large enough for numerical convergence. However, the number of terms must be small enough to provide continuous derivatives numerically. Up to 75 terms have been included in the results presented. For the triangular surfaces shown, a 25-term Fourier series is used to generate the surface profiles. Typical surface lengths are divided into 2400 increments. These lengths require the memory limit of each machine. Surfaces that have a large h/λ require more increments than surfaces with small $\lambda 1/\lambda$. All results presented conserve energy within 1 percent as evaluated by examining the conservation of energy for a dielectric surface (i.e., $K = 0.0$).

4. Numerical Results and Interpretations Concerning a Rough Surface-Case of a "V" Surface Illuminated by a Plane Wave

We applied our model to the case of a surface presenting a "V" roughness and illuminated by a monochromatic plane wave of wavelength $\lambda = 0.6328\mu m$, under the angle of incidence θ_0, for the two polarizations "p" and "s". This surface is made of barium sulphate ($BaSO_4$), with a complex refractive index of $n_C = 1{,}628 + 0,\ 0003$i, and it has cavities in the shape of a symmetrical or asymmetrical "V". Recall that

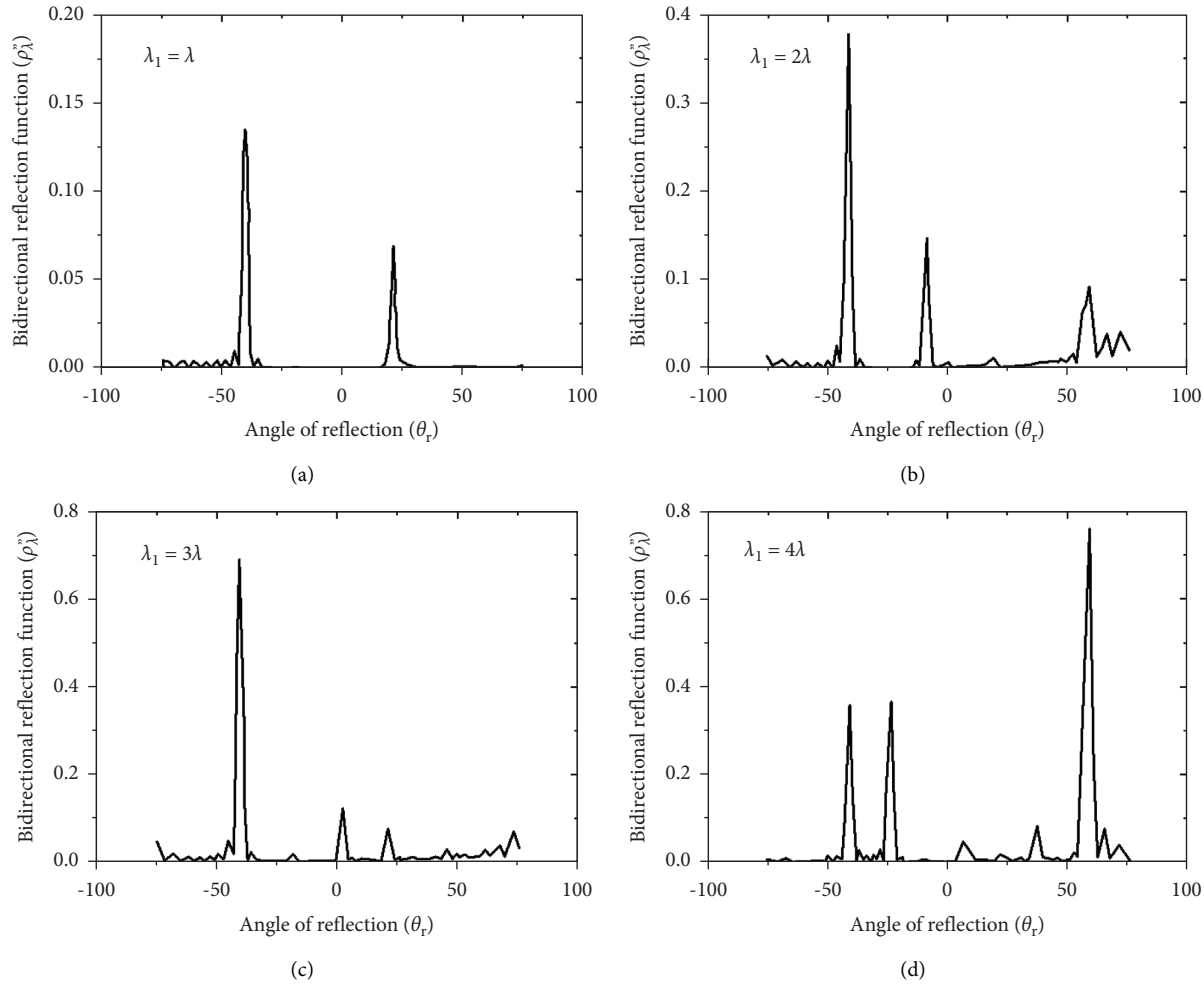

Figure 4: Bidirectional reflection function of polarization s. Influence of the geometric period ($\lambda = 0.6328\mu m, n_c = 1.628 + 0.0003i, \theta_0 = 20^0, h = \lambda, f_0 = 0.5$).

the profile of such a surface is characterized by its height h, its geometric period λ_1, and its peak position parameter f_0. We are primarily interested in the behavior of the bidirectional reflection function $\rho''_\lambda(\theta_0, \theta_r)$ with respect to the geometric parameters of the profile. Second, we examine the influence of the geometric period on the monochromatic directional emissivity of such a surface.

4.1. Influence of Geometric Parameters on $\rho''_\lambda(\theta_0, \theta_r)$. For a height h equal to the wavelength of the incident radiation, and a value fixed at 0.5 of f_0 ("V" symmetrical), we represent the variations of the bidirectional reflection function for values of the geometric period λ_1, respectively, equal to λ, 2 λ, 3 λ, and 4 λ, in each case of polarization. The representative curves show peaks of variations of different magnitudes, with, in each case, a predominant peak.

4.1.1. Case of "p" Polarization. In the context of the "p" polarization, it appears from Figures 3(a)–3(d) that the representative curves of $\rho''_\lambda(\theta_0 = 20^0, \theta_r)$ present a dominant peak of reflection corresponding to the angle of reflection $\theta_r = -42^0$. The amplitude of this peak goes from the value 0.12 to 0.55 when λ_1 varies from λ to 3λ; while it takes the value 0.34, or 2.8 times that of the dominant peak relative to $\lambda_1 = \lambda$, for $\lambda_1 = 4\lambda$.

The number of peaks increases when the geometric period increases, and it passes from two to seven peaks when λ_1 passes from λ to 4λ. This result is consistent with that provided by the diffraction theory of gratings with the same geometric shape as our surface.

4.1.2. Case of "s" Polarization. In the case of "s" polarization, Figures 4(a)–4(d) show that the geometric period λ_1 also varies with the number of reflection peaks, their positions, and the amplitude of the dominant peak. The same variation in the number of peaks, as previously, is observed. The dominant reflection angle corresponds to the maximum amplitude peak, and it is -42° for values of λ_1 equal to λ, 2λ, and 3 λ, while it is around 58° for $\lambda_1 = 4\lambda$. The value of $\rho''_\lambda(\theta_0 = -20^0, \theta_r = -42^0)$ is multiplied by 2.7 when λ_1 going from λ to 2λ and by 5 when λ_1 going to λ to 3λ; while it is equal to 0.75, 7 times that of the dominant peak relative to $\lambda_1 = \lambda$. The amplitude of the dominant peak is higher in the case of the "s" polarization than that corresponding to the "p" polarization.

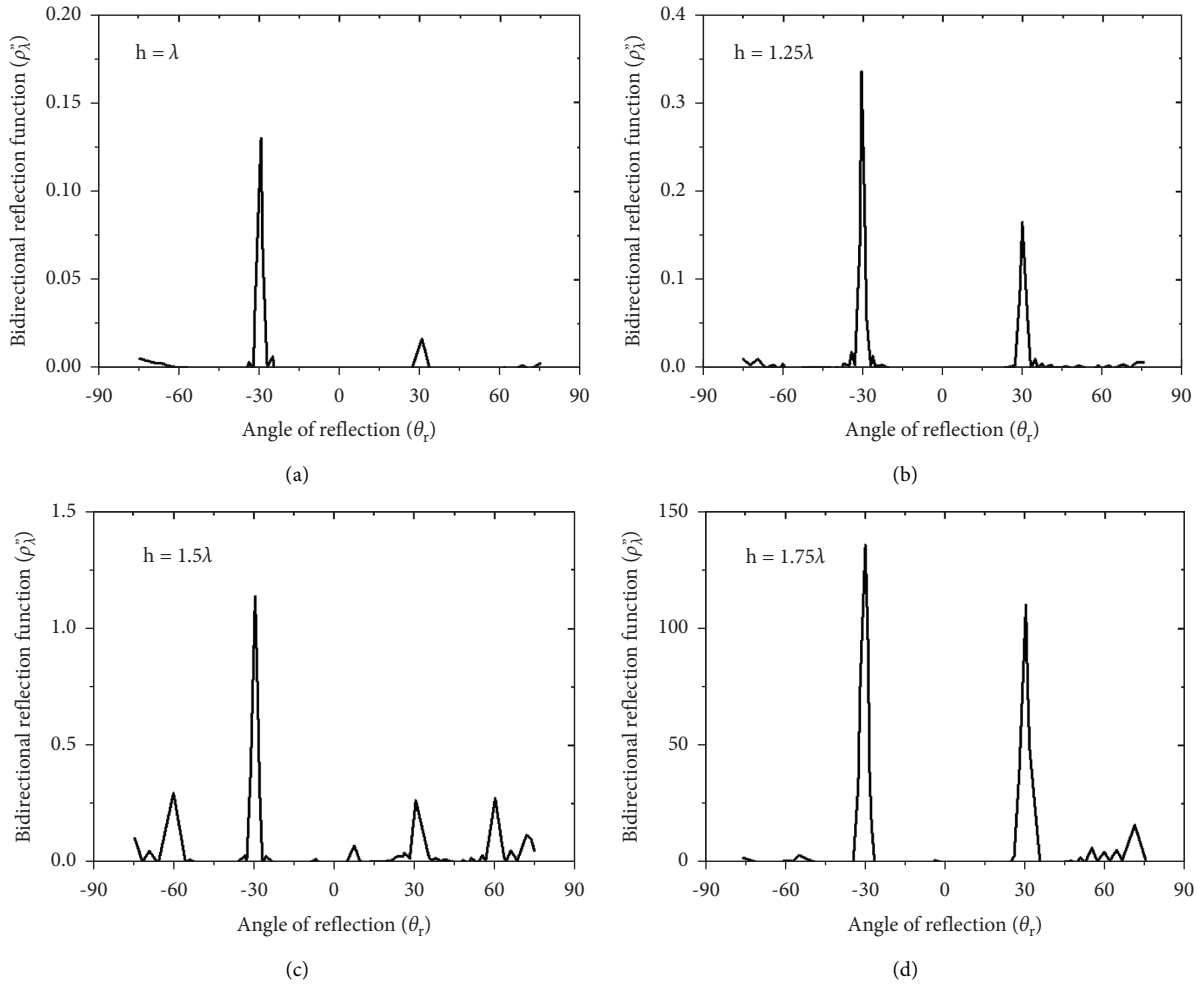

Figure 5: Bidirectional reflection function of polarization p. Influence of height h ($\lambda = 0.6328\mu m, n_c = 1.628 + 0.0003i, \theta_0 = 30^0, \lambda_1 = \lambda, f_0 = 0.5$).

4.2. Height Influence: h. We study the influence of the height h on the behavior of $\rho''_\lambda(\theta_0 = 30^0, \theta_r)$ by considering the cases corresponding to the values of h equal to λ, 1.25λ, 1.5 λ, 1.75λ, and a geometric period λ_1 equal to λ, in the two cases of polarization.

4.2.1. Case of "p" Polarization. Figures 5(a)–5(d), in the case of the "p" polarization, essentially highlight the existence of two dominant reflection peaks, one located around the direction and the other located around of direction $\theta_r = -30^0$, symmetrical to the first with respect to the normal. The amplitude of these peaks increases with h. We report that the flow diffused in an incoherent way and grows when h increases. In addition, note that the amplitude of the dominant antispecular peak, that is, corresponding to the direction $\theta_r = -30^0$, takes precedence in all these cases over the specular peak defined by $\theta_r = 30^0$. Note that these observations remain practically valid when we consider a ratio h/λ_1 less than unity, as shown in Figures 5(a)–5(d).

4.2.2. Case of "s" Polarization. In the case of the "s" polarization, the influence of the height h on $\rho''_\lambda(\theta_0 = 30^0, \theta_r)$ is illustrated using Figures 6(a)–6(d). We note that there, as in the previous case, exist two reflection peaks, one following the specular direction $\theta_r = 30^0$ and the other following the antispecular direction $\theta_r = -30^0$ and there is an increase in incoherent diffused flux as h increases. However, for h equal to 1.25λ where 1.75λ, the amplitude of the specular reflection peak is greater than that of the antispecular peak.

4.3. Influence of the Asymmetry of the Cavity. To illustrate the influence of the asymmetry of the cavities on the bidirectional reflection function, we have varied the height h and the geometric period λ for values of f_0 equal to 0.5, 0.7, and 0.9, in both cases of polarization. For the geometric period λ_1 equal to λ and the height h equal to 1.25λ, we note that the positions of the peaks, located at 30° (specular) and at −30° (antispecular), remain unchanged when f_0 varies. The amplitude of the antispecular peak increases remarkably when

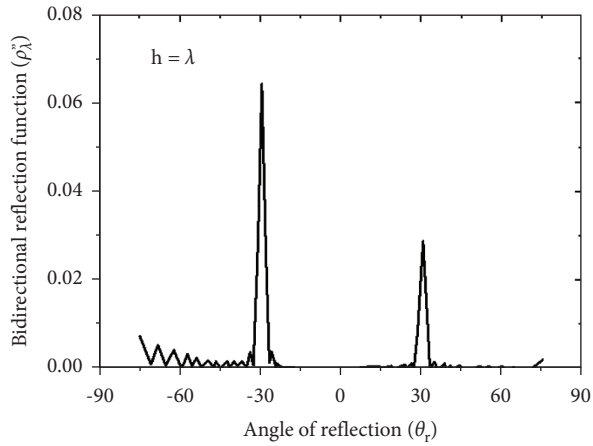

(a)

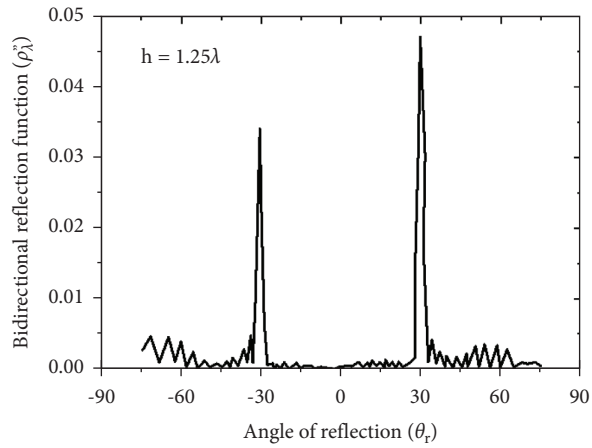

(b)

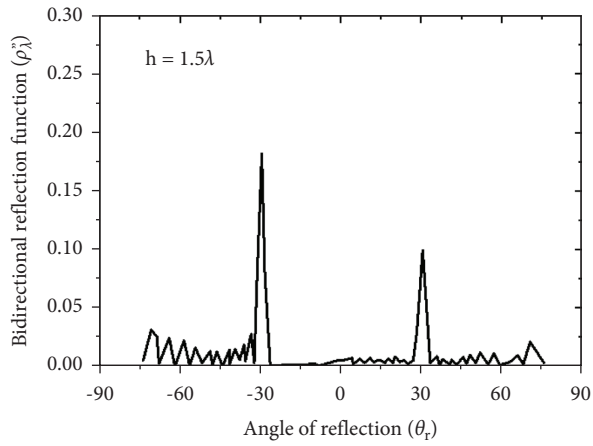

(c)

Figure 6: Continued.

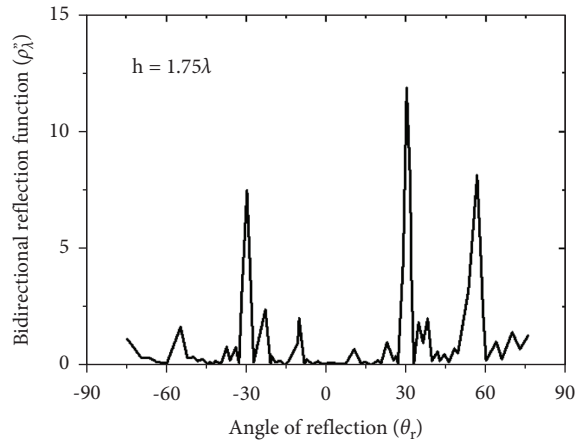

(d)

Figure 6: Bidirectional reflection function of polarization s. Influence of height h ($\lambda = 0.6328\mu m, n_c = 1.628 + 0.0003i, \theta_0 = 30^0, \lambda_1 = \lambda, f_0 = 0.5$).

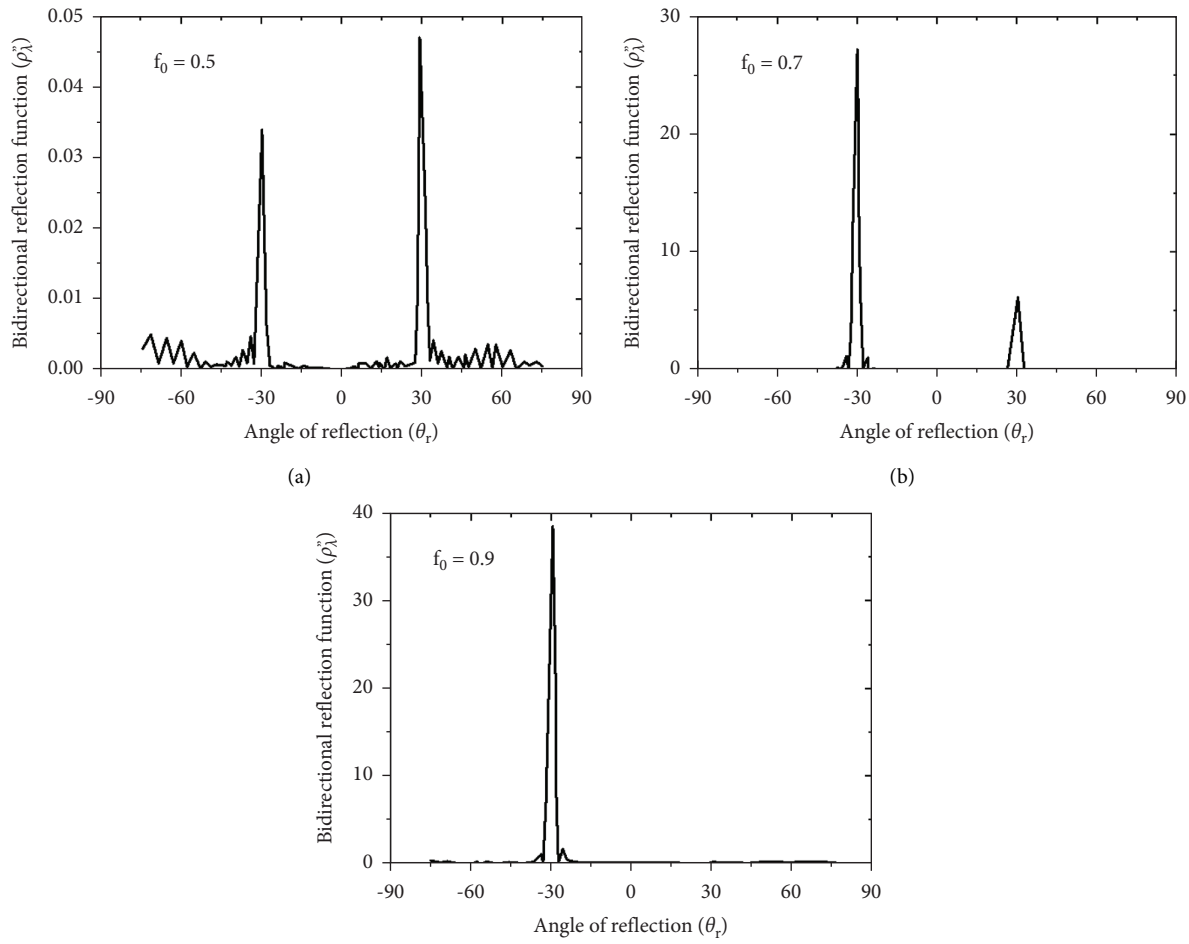

(a) (b)

(c)

Figure 7: Bidirectional reflection function of polarization S. Influence of dissymmetry of the cavity ($\lambda = 0.6328\mu m, n_c = 1.628 + 0.0003i, \theta_0 = 30^0, \lambda_1 = \lambda, h = 1,25\lambda$).

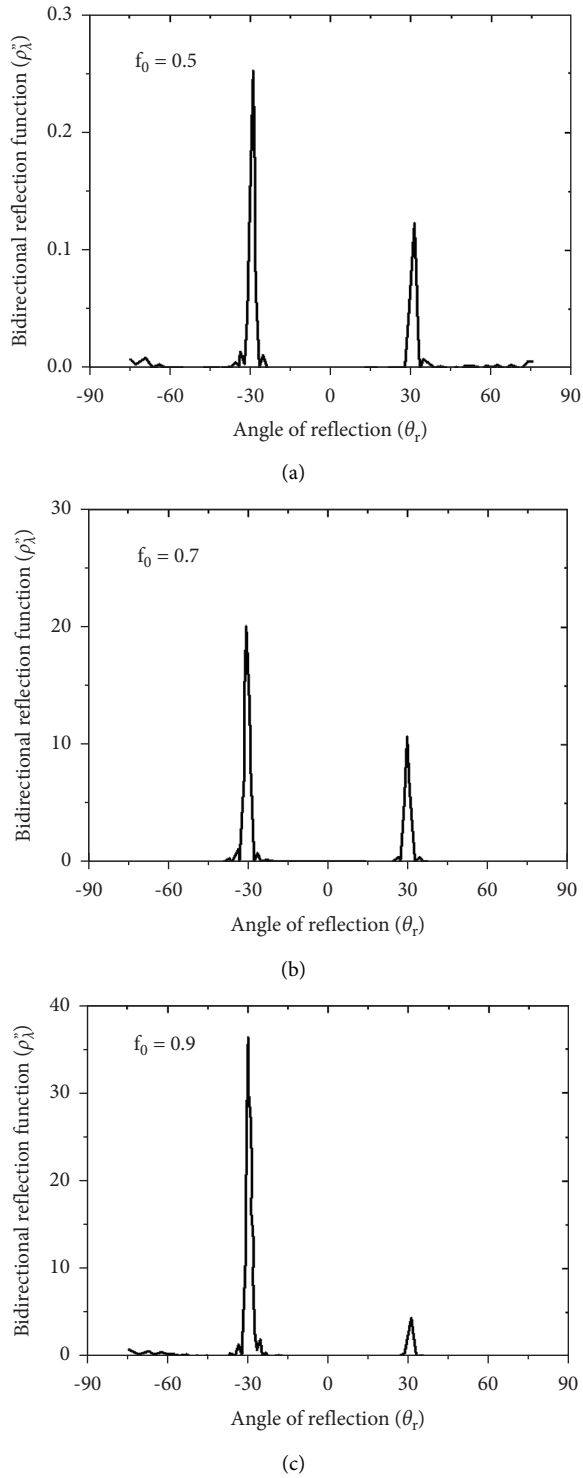

FIGURE 8: Bidirectional reflection function of polarization ``P'': influence of dissymmetry of the cavity ($\lambda = 0.6328\mu m, n_c = 1.628 + 0.0003i, \theta_0 = 30^0, \lambda_1 = \lambda, h = 1,25\lambda$).

f_0 goes from 0.5 (symmetrical "V") to 0.9; whereas that of the specular peak starts increasing when f_0 goes from 0.5 to 0.7, then decreases when f_0 reaches 0.9. The flux reflected in an antispecular way becomes more and more important than that reflected in the specular direction when the asymmetry increases.

These results are illustrated in Figures 7(a)–7(c) and 8(a)–8(c). Note also that the same results are valid for a height h and a geometric period λ_1 of the order of magnitude of the wavelength, in both cases of polarization. In Figures 9(a)–9(c) and 10(a)–10(c), we have represented the bidirectional reflection function for surfaces characterized

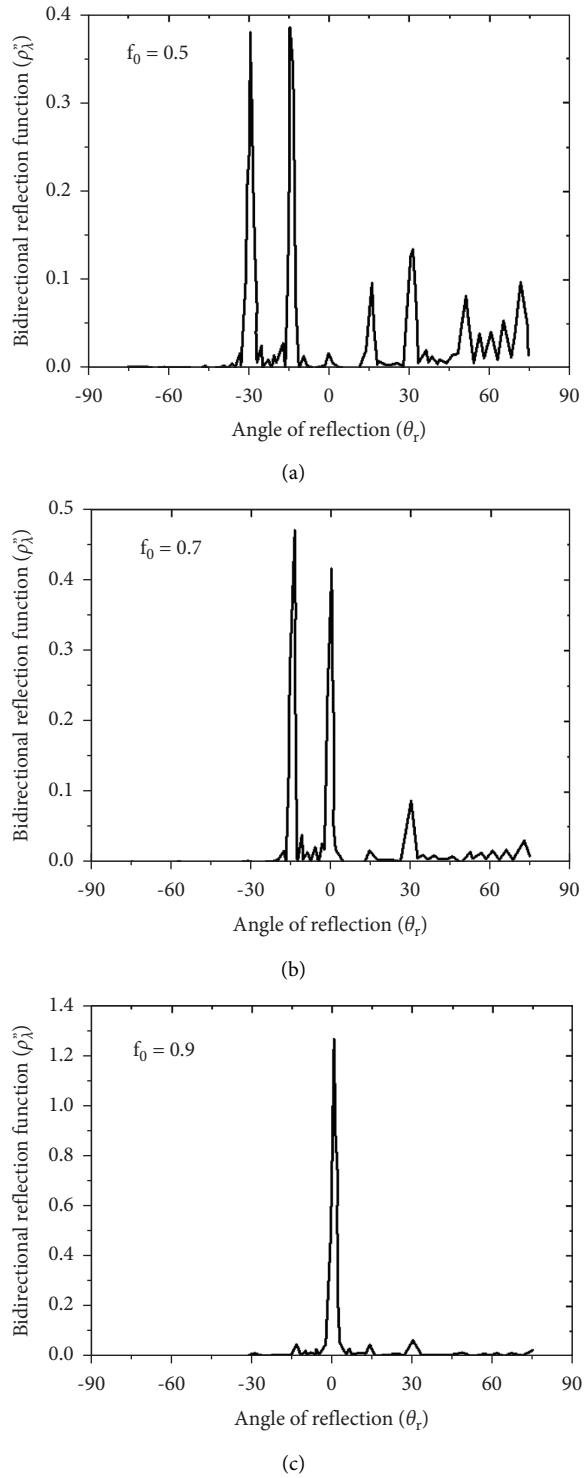

FIGURE 9: Bidirectional reflection function of polarization ``S``: influence of dissymmetry of the cavity ($\lambda = 0.6328\mu m, n_c = 1.628 + 0.0003i, \theta_0 = 30^0, \lambda_1 = \lambda, h = 1\lambda$).

by the parameters h equal to λ and λ_1 equal to 4λ, in the same cases of asymmetry as previously described, in "p" and "s" polarization. We note that the reflected flux following a certain number of peaks in the case of symmetrical cavity concentrates along the normal when the asymmetry reaches the value 0.9.

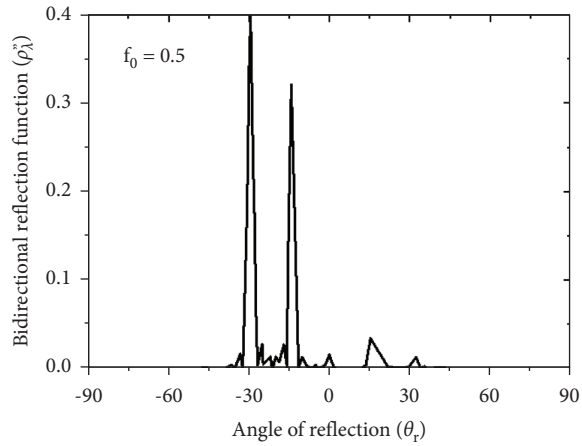

(a)

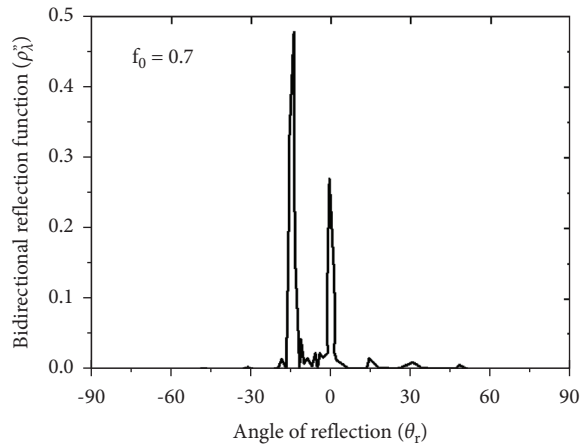

(b)

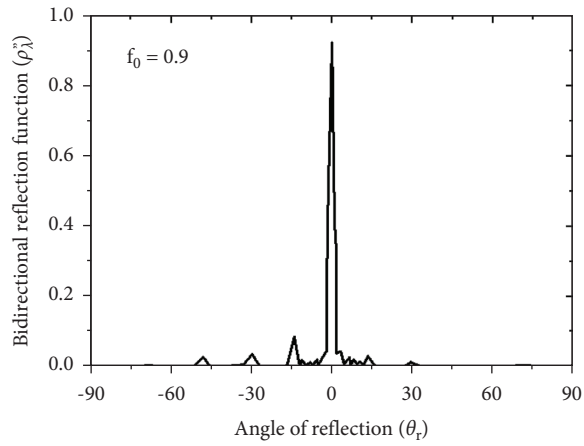

(c)

FIGURE 10: Bidirectional reflection function of polarization ``P``: influence of dissymmetry of the cavity ($\lambda = 0.6328\mu m, n_c = 1.628 + 0.0003i, \theta_0 = 30^0, \lambda_1 = \lambda, h = 1\lambda$).

4.4. Emissivity

4.4.1. Influence of the Geometric Period. In Figures 11(a)–11(d), we represent the directional surface emissivity presenting cavities in the shape of a symmetrical "V" ($f_0 = 0, 5$), of the same height h equal to λ and of respective geometric periods 4λ, 3λ, 2λ, and λ, in both cases of polarization. Note that for a smooth flat surface of the same material ($BaSO_4$), the emissivity is close to unity along directions up to 60° around the normal, and it then decreases for grazing directions. As we might expect, we see a slight increase in emissivity for directions up to

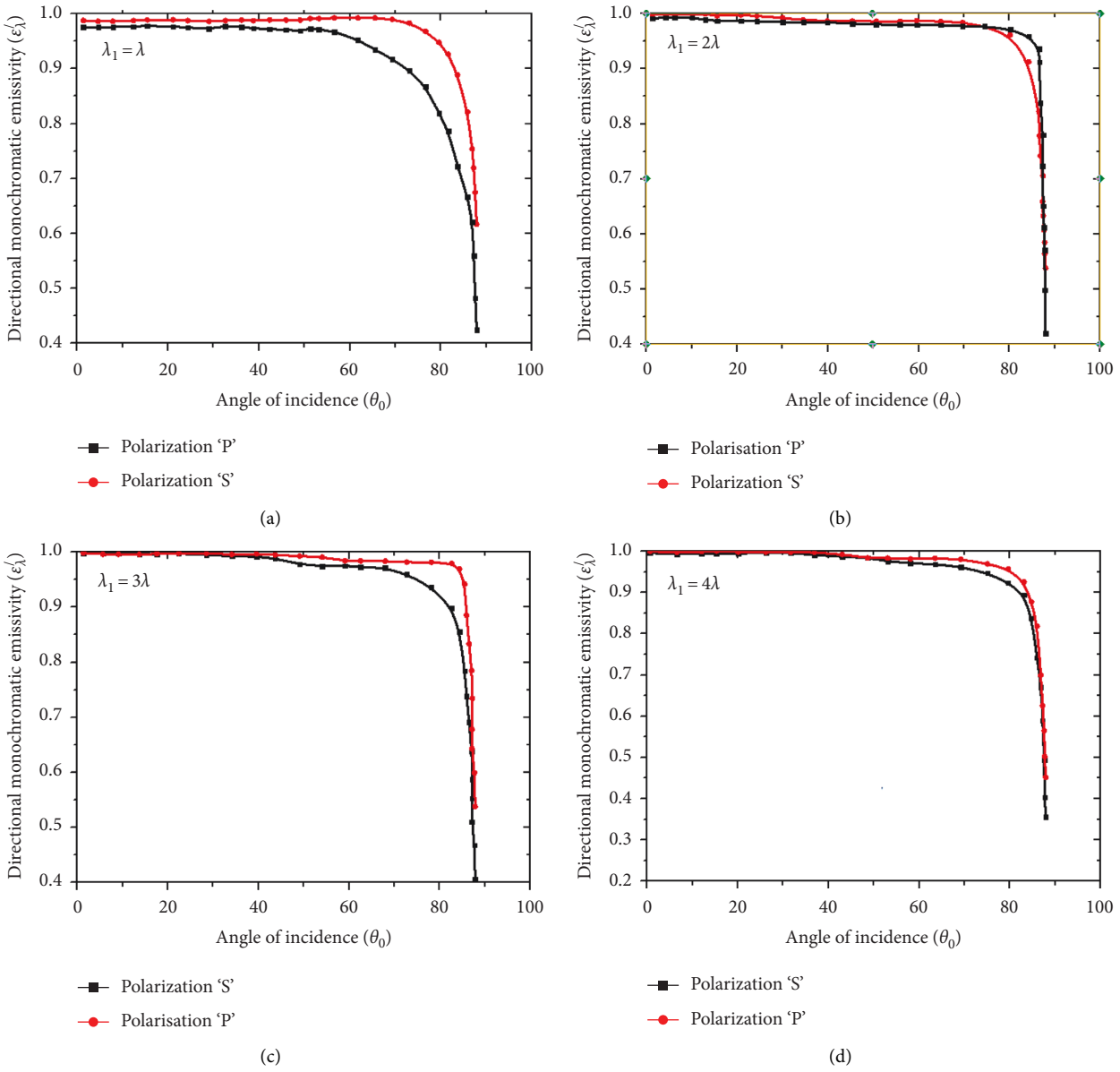

FIGURE 11: Directional emissivity monochromatic polarization p and s: influence of the geometric period ($\lambda = 0.6328\mu m, n_c = 1.628 + 0.0003i, h = \lambda, f_0 = 0.5$).

grazing directions as the geometric period decreases. Indeed, this is consistent with the effect of the same roughness on the emissivity for a surface made of a material of the same nature [16].

5. Conclusion

This work allowed us to determine the radiative properties of rough surfaces from the electromagnetic theory by the surface integral method. The exploitation of computer codes, in the case of a triangular-shaped surface, led to the study of the influence of geometric parameters on the bidirectional reflectivity as well as on the emissivity of these surfaces. The results obtained are in an agreement with those provided by the theory of diffraction or by other research works in the treated case. Furthermore, we point out that the surface integral method becomes very expensive numerically as soon as the modulus of the complex refractive index of the medium increases.

Nomenclature

P_{inc}: Incident flow
$r_p(\theta_r)$: Polarization reflection function "p"
$r_s(\theta_r)$: Reflection function in polarization "s"
$\widetilde{V}$: Volume located in Ω_1
V: Volume located in Ω_2
λ_1: Geometric period
Ω_2: Dielectric medium
ω: Incident wave pulsation

Ω_1: The void
ξ: Surface profile
$\varepsilon(\omega)$: Dielectric function
λ: Wave length
θ: Angle of incidence or reflection
δ: Dirac
γ: Normalization constant
ρ_s'': Bidirectional reflection function in "s" polarization
μ: Magnetic permeability of the medium
μ_0: Vacuum permeability
ε_0: Vacuum permittivity
$\overrightarrow{E}$: Electric field
$\overrightarrow{H}$: Magnetic excitation field
f_0: Peak position of the "V" surface profile
G: Green's function
$H_0^{(1)}$: Zero-order Hankel function of the first kind
$\overrightarrow{H}^*$: Conjugate of the magnetic field
h: Height of the "V" surface profile
$\overrightarrow{K}$: Wave vector
n_C: Complex index
p; TM: Magnetic transverse polarization
s, TE: Electrical transverse polarization
P_{diff}: The stream diffused through the plane $z = \text{constant}$ located above the profile
$\partial\widetilde{V}$: Closed surface that limits the volume $\widetilde{V}$
∂V: Firm surface which limits the volume V
$\langle \overrightarrow{S} \rangle$: Mean value of the Poynting vector
ρ_p'': Bidirectional reflection function in polarization "p".

Data Availability

Data are available on request.

Conflicts of Interest

The author declares that there are no conflicts of interest.

References

[1] M. F. Modest, "Three dimensional radiative exchange factors for nongray, nondiffuse surfaces," *Numerical Heat Transfer*, vol. 1, pp. 403–416, 1978.

[2] V. Nieto and J. M. Soto-Crespo, "Monte Carlo simulation for scattering of electromagnetique waves from perfectly random rough surfaces," *Optics Letters*, vol. 12, pp. 979–981, 1987.

[3] J. A. S. Gil and M. Nioto-Vesprinas, "Lights scattering from random rough dielectric surfaces," *Journal of the Optical Society of America A*, vol. 8, no. 8, pp. 1270–1286, 1991.

[4] A. A. Maradudin, T. Michel, A. R. McGurn, and E. R. Mendez, "Enhanced backscattering of light from a random grating," *Annals of Physics*, vol. 203, no. 2, pp. 255–307, 1990.

[5] J. J. Grefet, "Scattering of s-polarised electromagnetic waves by 2D obstacle near an interface," *Optics Communications*, vol. 72, no. 5, pp. 274–278, 1989.

[6] J. J. Greffet and F.-R. Ladan, "Comparison between theoretical and experimental scattering of an s-polarized electromagnetic wave by a two-dimensional obstacle on a surface," *Journal of the Optical Society of America A*, vol. 8, no. 8, pp. 1261–1269, 1991.

[7] R. A. Ladan and R. O. Buckius, "Electromagnetic theory predictions of the directional scattering from triangular surfaces," *Journal of Heat Transfer*, vol. 116, no. 3, pp. 639–645, 1994.

[8] M. J. Buckius, J. C. Dainty, M. J. Kim, J. C. Dainty, A. T. Fiberg, and A. J. Sant, "Experimental study of enhanced bask scattering from one-and two dimensional random rough surfaces," *Journal of the Optical Society of America A*, vol. 7, pp. 569–577, 1990.

[9] T. R. Michel, M. E. Knotts, and K. A. O'Donnell, "Stokes matrix of a one-dimensional perfectly conducting rough surface," *Journal of the Optical Society of America A*.vol. 9, no. 4, pp. 585–596, 1992.

[10] D. Maystre, "Integral methods," *Electromagnetic Theory of Gratings*, Springer-Verlag, Berlin, Germany, 2019.

[11] M. Abramowitz and I. A. Stegun, *Handbook of Mathematical Function*, Courier Corporation, North Chelmsford, MA, USA, 1965.

[12] S. R. Charles, S. M. Shah, and C. V. Stanjevic, *Theory and Applications of Fourier Analysis*, Marcel Dekker, New York, NY, USA, 1981.

[13] M. Nieto-Vesperinas, *Scattering and Diffraction in Physical Optics*, Instituto de Research Council (CSIC), Madrid, Spain, 1991.

[14] J.-J. Greffet and R. Carminati, "Radiative transfer at nanometric scale: are the usual concepts still valid?" *Heat and Technology*, vol. 18, p. 81, 2000.

[15] J.-J. Greffet, R. Carminati, K. Joulain, J. P. H. Mulet, S. Mainguy, and Y. Chen, "Coherent emission of light by thermal sources," *Nature*, vol. 416, no. 6876, pp. 61–64, 2002.

[16] R. A. Dimenna and R. O. Buckius, "Microgeometrical contour contributions to surface scattering," *Thermal Science and Engineering*, vol. 2, pp. 166–171, 1994.